CrystEngComm

Accepted Manuscript

ROYAL SOCIETY OF CHEMISTRY

www.rsc.org/crystengcomm

Growth of oriented $Bi_{40-x}In_xTe_{60}$ (x=3, 7) thermoelectric material by seeding zone melting for the enhancement of chemical homogeneity

Dongmei Liu[1]*, Hannes Engelhardt[1], Xinzhong Li[1,2], A. Löffler[1], Markus Rettenmayr[1]

[1]Otto Schott Institute of Materials Research, Friedrich Schiller University, Löbdergraben 32, D-07743 Jena, Germany

[2] School of Materials Science and Engineering, Harbin Institute of Technology, 150001 Harbin, PR China

Abstract: A zone melting technique with seeding has been developed to prepare oriented $Bi_{40-x}In_xTe_{60}$ (at%, x=3;7) thermoelectric material with enhanced chemical homogeneity. The respective initial compositions of sample and seed were chosen according to the pseudo-binary Bi_2Te_3-In_2Te_3 phase diagram that was experimentally redetermined with the aid of a former mushy zone that was resolidified in a temperature gradient. Oriented $Bi_{40-x}In_xTe_{60}$ bulk material with a uniform composition close to the target value over the entire length of the zone-melted region along the growth direction has been successfully manufactured.

*Corresponding author: Tel.:+49(0)3641-947798
E-mail address: dongmei.liu@uni-jena.de (Dongmei Liu)

1. Introduction

Bismuth telluride (Bi_2Te_3) crystallizes in a rhombohedral lattice and exhibits a layered structure consisting of five individual atomic layers in the sequence Te(1)-Bi-Te(2)-Bi-Te(1) perpendicular to the c-axis in the unit cell. Bi_2Te_3-based materials are the most prominent thermoelectric materials operating near room temperature. Possible methods for producing Bi_2Te_3-based materials include different varieties of directional solidification, and powder sintering using milling, hot pressing and so on. Among these methods, directional solidification, based on e.g. zone melting, Bridgman and Czochralski growth can produce a thermoelectric material exhibiting better thermoelectric properties than their counterparts prepared by the other methods. This is due to the effective exploitation of the specific anisotropy in the thermoelectric properties generated from the layered structure of the Bi_2Te_3 crystal, of which the transport properties are best optimized perpendicular to the <001> direction [1-3]. Such advantage of directional solidification techniques for anisotropic thermoelectric materials to improve performance has been confirmed again in SnSe system, in which an unprecedented figure of merit zT=2.6 has been obtained in SnSe single crystals synthesized by the Bridgman method [4]. However, owing to convection instabilities in the melt and to the related inhomogeneous solute redistribution processes during crystal growth, chemical homogeneity in the Bi_2Te_3-based oriented material is not easy to accomplish [5-11]. Such chemical inhomogeneity introduces a variation of site occupancy in the grown crystal that entails locally less favorable thermoelectric properties or even transformation of conductivity type from positive to negative along growth direction in a bulk ingot [10], which would lead to loss of the desired thermoelectric properties.

In the present work, a tailored zone melting technique is presented in which a seeding alloy is used to regulate the solute redistribution during zone melting, with the aim to prepare bulk oriented Bi_2Te_3-based

samples with a constant composition over the entire length of the sample. The Bi_2Te_3-In_2Te_3 system, in which a multi-scale hierarchical structure from atomic doping [12-14] to nanoscale [15, 16] to mesoscale [17] and the accompanying enhanced thermoelectric properties can be generated, is chosen. It is important to note that the thermoelectric properties of $Bi_{40-x}In_xTe_{60}$ (at%) are very sensitive to the In concentration in the range from 0 to 7 at% [18], and that inversion of the conductivity type from positive to negative is expected in crystals grown by conventional directional solidification techniques, as it has been observed for Bi_2Te_3 crystals [10]. Hence, it is indispensable to precisely control the composition in $Bi_{40-x}In_xTe_{60}$ crystals.

The selection of the composition of the seed crystal for a chosen target composition of the thermoelectric material is crucial in the seeding zone melting technique. Prior work on this alloy system has focused on the maximum solubility of In in Bi_2Te_3 which is confirmed to be ~8at% [19, 20], and in the quite limited available pseudo-binary Bi_2Te_3-In_2Te_3 phase diagrams [20, 21] there are conflicting data concerning the solubility of In_2Te_3 in Bi_2Te_3. Hence, the liquidus and solidus lines in the Bi_2Te_3-rich part of the pseudo-binary phase diagram of the Bi_2Te_3-In_2Te_3 system were first experimentally re-assessed using the temperature and concentration distribution in a former mushy zone that resolidified in a temperature gradient [22-27].

2. Experimental

2.1 Annealing of mushy zone in a temperature gradient

For obtaining the major part of the solidus and liquidus lines of the pseudo-binary Bi_2Te_3-In_2Te_3 phase diagram, two Bi-In-Te alloys, particularly $Bi_{33}In_7Te_{60}$ and $Bi_{28}In_{12}Te_{60}$ (at%), were subjected to temperature gradient thermal annealing experiments. $Bi_{28}In_{12}Te_{60}$ is expected to be in the hypoeutectic composition range. As-cast ingots were produced from pure Bi, Te and In by induction melting in vacuum

sealed quartz, during which strong convection in the melt was stimulated to guarantee overall homogeneity of the as-cast ingot. The dimensions of the samples were ~10 mm in diameter and ~90 mm in length. As-cast rods were then exposed to a steep temperature gradient. A schematic illustration of the experimental set-up is shown in Fig. 1(a). One end of the sample was heated to a temperature above the liquidus temperature, the other end kept below the solidus temperature, leading to the formation of a mushy zone between the non-melted as-cast zone and the completely melted liquid zone, as illustrated in Fig. 1(b). The mush was held in the temperature gradient for 4 hours to reach complete resolidification of the mushy zone. Due to thermodynamic equilibration in the temperature gradient and the accompanying formation of concentration gradients, upward solute diffusion and further processes as e.g. temperature gradient zone melting (TGZM) occur, and the mushy zone transforms to a completely solid zone with a solute concentration that follows the local solidus concentration [22-27]. After complete resolidification of the mushy zone, a longitudinal section of the rod was ground and polished, microstructure and composition distribution along the axis direction were determined using a scanning electron microscope (SEM) equipped with energy dispersive spectroscopy (EDS).

2.2 Seeding zone melting

In the present work, a seeding zone melting was developed aiming to produce $Bi_{33}In_7Te_{60}$ and $Bi_{37}In_3Te_{60}$ (at%) oriented homogeneous ingots. The seeding zone melting experiments were performed in an experimental set-up that is very similar to that shown in Fig. 1(a). For the zone melting, the ingot consisted of two parts, the seed ingot and the sample ingot, as illustrated in Fig. 1(c). The overall compositions of the sample, C_S, and of the seed alloy, C_S/k, (where k is the solute redistribution coefficient), respectively, were chosen based on the data obtained by the annealing experiments in the temperature gradient. Crystal growth at the trailing edge of the melted zone was processed from the

seeding ingot to the sample ingot. During zone melting, the liquid zone was melted by high frequency induction heating, which at the same time stimulates convection in the liquid through Lorentz forces and lateral temperature gradients, so that a uniform solute concentration distribution in the liquid zone is achieved. Heating and cooling zone are separated by adiabatic Al_2O_3 plates. The quartz crucible was initially placed in the system such that the boundary between the seed and sample ingots was located at the top interface between the heating zone and the cooling zone, as shown as the stage I in Fig. 1(c). Hence, the zone melting growth proceeds from the seed ingot to the sample ingot. After initial melting, thermal holding for 60 min followed to ensure a planar solid/liquid interface on which uniform crystal growth can be attained. Following these steps, the liquid zone was pulled through the sample at the desired pulling velocity of 2μm/s for a freezing distance of 30mm. With the proceeding molten zone, a part of the sample ingot of composition C_S melts, and simultaneously the same length of solid phase of equal composition C_S solidifies, as shown as the stage II in Fig. 1(c). Hence, the concentration in the molten zone remains at C_S/k, at all times, guaranteeing continuous precipitation of solid phase of the composition C_S. An inset picture of a typical crystal obtained via such seeding zone melting is shown in Fig. 1(c).

A longitudinal section of the zone-melted rod was ground and polished. X-ray diffraction (XRD) was applied for phase analysis in the zone-melted region. Microstructure and composition distribution along the axis direction were analyzed in the same manner as mentioned above.

3. Results and discussion

During temperature gradient thermal annealing experiments of $Bi_{40-x}In_xTe_{60}$ (x=7, 12) alloys (i.e. after 4-hour thermal stabilization) the former mushy zone between the as-cast region and the molten zone transforms into a single Bi_2Te_3 region, as shown by the in-set microstructure in Fig. 2, of which the

corresponding temperature of the upper interface is the melting point of the alloy T_L, and that of the lower interface is the solidus temperature T_S. The measured concentration of In across this completely resolidified mushy zone and the temperatures those are assigned to the measurement position are shown by the black circles in Fig. 2. Based on the experimental results and relating to previous literature on pseudo-binary Bi_2Te_3-In_2Te_3 phase diagram [20, 21], the solidus and liquidus lines are assumed to be straight lines. Consequently, the solidus line of the Bi_2Te_3 rich side of the pseudo-binary Bi_2Te_3-In_2Te_3 phase diagram is approximated by a linear least square fit, as illustrated by the blue line in Fig. 2. The average concentrations of the solid C_S and liquid phase C_L across the quenched solid/liquid interface (T_L) were measured, yielding the partition coefficient, $k=C_S/C_L$. For the thermal annealing experiment on $Bi_{33}In_7Te_{60}$, the In concentration of the solid at the T_L interface was about 3.0 ±0.5 at% and a value of k=0.43±0.07 was calculated. For the $Bi_{28}In_{12}Te_{60}$ alloy, the In concentration of the solid at the T_L interface was 6.2±0.5 at% and a value of k=0.52±0.04 was calculated. In the following, a constant value of being covered by the two independent measurements is used, particularly k=0.48. It is worth noting that the In concentration at the lowest interface of the resolidified single phase Bi_2Te_3 region of $Bi_{28}In_{12}Te_{60}$, i.e. the maximum solubility of In in Bi_2Te_3, was measured to be 8.0±0.5 at%. Considering the experimental measured In concentration range, from 3.0 to 8.0 at%, taking over the majority of the total solidus of the Bi_2Te_3 rich part of the pseudo-binary Bi_2Te_3-In_2Te_3 phase diagram, the two measured values of k were used to determine a possible range of liquidus concentrations that correspond to the respective solidus concentrations by dividing the fitted solidus concentration by k, as illustrated by the grey region in Fig. 2. The experimentally assessed phase diagram is more close to that determined by Scherpereel et al in 1968 [20]. Several compositions of the solidus and liquidus line deduced from Ref 16 are shown as squares in Fig. 2.

Based on the experimental data of the pseudo-binary Bi_2Te_3-In_2Te_3 phase diagram, $Bi_{33}In_7Te_{60}$ and $Bi_{37}In_3Te_{60}$ (at%) were grown by zone melting with seeding, and the concentration along the crystal growth direction was measured. The composition $Bi_{26.5}In_{13.5}Te_{60}$ (at%) was selected as the concentration of the seeding alloy for $Bi_{33}In_7Te_{60}$ (at%), and $Bi_{33}In_7Te_{60}$ (at%) for $Bi_{37}In_3Te_{60}$ (at%). During zone melting, the pulling velocity was chosen as 2μm/s to maintain a plain front throughout the growth process. Fig. 3 shows backscattered electron images of $Bi_{33}In_7Te_{60}$ after conventional zone melting, i.e. without seed alloy, and after zone melting with seeding. Single phase Bi_2Te_3 in the zone-melted region and growth with a planar solid/liquid interface are confirmed. In the XRD pattern of the zone-melted sample, as shown in Fig. 3 (f), apparently, the peak (0 0 $\underline{15}$) of Bi_2Te_3 is the strongest peak and the other two peaks (0 0 $\underline{18}$) and (0 0 $\underline{21}$) are much weaker. Compared with the standard isotropic pattern of Bi_2Te_3 in which the peak (0 1 5) is the strongest, the intensity of the peak (0 0 $\underline{15}$) of Bi_2Te_3 is much higher. The XRD results suggest that the zone-melted samples, $Bi_{37}In_3Te_{60}$ and $Bi_{33}In_7Te_{60}$, exhibit a preferential orientation of a {001} plane parallel to the growth axis, allowing a full exploration of the thermoelectric property anisotropy of this material [1-3].

The composition in the zone-melted ingots along the growth direction is plotted as a function of the freezing distance from the bottom end (in Fig. 4). For the $Bi_{33}In_7Te_{60}$ ingot after conventional zone melting, with increasing freezing distance up to 30mm the In concentration increases from ~3.5 at% to ~5 at%. After employing the seed alloy $Bi_{26.5}In_{13.5}Te_{60}$, the In concentration in the zone-melted ingot is close to the target level of ~7.0at% in almost the entire zone-melted region. For the second alloy ($Bi_{37}In_3Te_{60}$), seeding also proved to be successful, as the In is homogeneously distributed in the zone-melted ingot with a concentration close to 3 at%.

A comparison on the composition distribution of the grown crystal prepared by the seeding zone melting

and the other traditional crystal growth methods are summarized in Table 1. For alloys with a large solidification interval and a solute redistribution coefficient k distinctly different from unity, as e.g. Bi_2Te_3-In_2Te_3, when prepared by Czochralski, Bridgman and zone melting, a pronounced composition gradient must form in the initial transient region before the steady-state is established and solidification occurs with constant composition [5-11]. The final transient is associated with the solute pile-up in front of the growing interface that eventually will solidify with a higher concentration. The length L_i of the initial transient region can be calculated according to [28]

$$L_i = \frac{4D}{kV}, \quad (1)$$

where D is solute diffusion coefficient in the liquid and V is the growth rate.

During preparation of a thermoelectric crystal via such methods, the growth rate is generally very low to guarantee planar growth of the crystal. This will lead to a relative long initial transient zone, especially for alloy systems with relatively small k values. It has been reported that the initial transient even occupied the first quarter length of the prepared Bi_2Te_3-Se_2Te_3 crystal via zone melting method [7]. Moreover, when produced by such methods, convection in the melt must be suppressed for reliable and reproducible results, which in practice is hard to accomplish. The existence of convection in most cases is connected with a non-uniform concentration and the non-existence of steady-state growth. When produced by seeding zone melting, the initial transient zone can be eliminated by proper selection of the seed alloy, and a uniform composition close to the target value is obtained over the entire length of the zone-melted region. During this seeding zone melting process, the necessary strong convection in the melt is far easier to achieve in practice than pure diffusion control.

For the $Bi_{40-x}In_xTe_{60}$ crystals, the thermoelectric properties are very sensitive to the In concentration in the range from 0 to 7at%, and an inversion of the conductivity type from positive to negative occurs at a

composition of ~2at% In [18]. Hence, it is especially necessary to precisely control the In composition of the $Bi_{40-x}In_xTe_{60}$ crystals to generate the desired thermoelectric properties. Additionally, the introduction of nanoscaled In-rich precipitates (of several nanometers in size) [15] or mesoscale In_2Te_3 precipitates of an extension between 0.1 and 1μm [17] as secondary precipitates via solid state transformation has the potential to enhance the thermoelectric properties of this material via a multi-scale hierarchical structure. Such an enhancement strategy requires a fundamental understanding of the relations between the structure and thermoelectric properties of these materials. This understanding has up to present not been worked out, because bulk oriented homogeneous Bi_2Te_3 crystals were not available. In this view, the seeding zone melting technique can not only contribute to the optimization of thermoelectric properties of Bi-In-Te based materials by simultaneously exploiting the anisotropy in the thermoelectric properties and improving the chemical homogeneity, but also shed light on fundamental questions concerning the control of meso- and nanoscale structures in the intermetallic phases which in turn will stimulate further enhancement of thermoelectric performance.

4. Conclusion

In the present work, based on accurate phase diagram data a crystal growth method applying seeding and zone melting is established to prepare oriented Bi_2Te_3 crystals as a thermoelectric material with optimized chemical homogeneity. The method, from the determination of the phase diagram to the seeding zone melting process, in principle can be applied to other thermoelectric materials, irrespective of crystal anisotropy, either improving thermoelectric performance of the respective ingots and/or allowing a more profound understanding of structure evolution of thermoelectrics.

References

[1] H. J. Goldsmid, *J. App. Phys.*, 1961, **32**, 2198.

[2] T. Caillat, L. Gailliard, H. Scherrer, S. Scherrer, *J. Phys. Chem. Solids*, 1993, **54**, 575.

[3] M. Carle, P. Pierrat, C. Lahalle-Gravier, H. Scherrer, S. Scherrer, *J. Phys. Chem. Solids*, 1995, **56**, 201.

[4] L. D. Zhao, S. H. Lo, Y. S. Zhang, H. Sun, G. J. Tan, C. Uher, C. Wolverton, V. P. Dravid, M. G. Kanatzidis, *Nature*, 2014, **508**, 373.

[5] F. König, *Cryst. Res. Technol.*, 1998, **33**, 219.

[6] G. Kavei, M. A. Karami, *Mater. Res. Bull.*, 2008, **43**, 239.

[7] M. Allahkarami, L. Seyed-Faraji, G. Kavei, Y.Zare, *Mater. Chem. Phys.*, 2010, **119**, 145.

[8] V. S. Zemskov, A. D. Belaya, U. S. Beluy, G. N. Kozhemyakin. *J. Cryst. Growth*, 2000, **212**, 161.

[9] G. N. Kozhemyakin, D. V. Lutskiy, M. A. Rom, P. V. Mateychenko, *J. Cryst. Growth*, 2009, **311**, 1466.

[10] K. A. Kokh, A. V. Makarenko, V. A. Golyashov, O. A. Shegai, O. E. Tereshchenko, *CrystEngComm*, 2014,**16**,581.

[11] D. Perrion, M. Chitroub, S. Scherrer, H. Scherrer, *J. Phys. Chem. Solids*, 2000, **61**, 1687.

[12] H. J. Goldsmid, *Pro. Phys. Soc.*, 1958, **71**,633.

[13] N. B. Brandt, V. A. Kulbachinskii, *Semicond. Sci. Technol.*, 1992, **7**, 907.

[14] S. B. Ovsyannikov, V. V. Shchennilov, G. V. Vorontsov, A. Y. Manakov, A. Y. Likhacheva, V. A. Kulbachinskii, *J. Appl. Phys.*, 2008, **104**, 053713

[15] Y. Zhai, T. Zhang, Y. Xiao, J. Jiang, S. Yang, G. Xu. *J. Alloys Comp*., 2013, **563**, 285.

[16] N. Peranio. Structural, chemical, and thermoelectric properties of Bi_2Te_3 Peltier materials: bulk, thin films, and superlattices. PhD thesis, Eberhard-Karls-Universität Tübingen, Germany, 2008.

[17] Nicholas A. Heinz, Teruyuki Ikeda, G. Jeffrey Snyder, *Acta Mater.*, 2012, **60**, 4461.

[18] S. KARAMAZOV, P. LOŠŤÁK, J. HORÁK, R. KUŽEL, *Phys. Stat. Sol. (a)*, 1995, **148**, 229.

[19] A. J. Rgsenberg, A. J. Strauss, *Phys. Chem.Solids*, 1961, **19**, 105.

[20] L. R. Scherpereel, P. L. Palumbo, E. A. Peretti, *J. Less-Common Metals*, 1968, **14**, 41.

[21] D. P. Belotskii, S. M. Dodik, I. N. Antipov, Z. I. Nefedova, *Ukrainskii Khimicheskii Zhurnal*, 1970, 3**6**, 897.

[22] H. Nguyen Thi, B. Drevet, J. M. Debierre, D. Camel, Y. Dabo, B. Billia, *J. Cryst. Growth*, 2003, **253**, 539.

[23] M. Buchmann, M. Rettenmayr. *J. Cryst. Growth*, 2005, **284**, 544.

[24] U. Bösenberg, M. Buchmann, M. Rettenmayr. *J. Cryst. Growth*, 2007, **304**, 281.

[25] Y. Q. Su, D. M. Liu, X. Z. Li, L. S. Luo, J. J. Guo, H. Z. Fu. *J. Cryst. Growth*, 2010, **312**, 2441.

[26] D. M. Liu, Y. Q. Su, X. Z. Li, L. S. Luo, J. J. Guo, H. Z. Fu. *J. Cryst. Growth*, 2010, **312**, 3658.

[27] H. Engelhardt, B. Hallstedt, M. Drüe, A. Löffler, M. Schick, M. Rettenmayr, *Adv. Eng. Mater*., 2013, **14**, 319.

[28] V. G. Smith, W. A. Tiller, J. W. Rutter. *Can. J. Phys.*, 1955, **33**, 723.

Acknowledgments

Financial support by the German Research Foundation (DFG) for two of the authors (HE and AL) under grant Re1261/7 is gratefully acknowledged.

Figure caption:

Fig. 1 Schematic illustrations of (a) experimental set-up and (b) determination of phase diagram via temperature gradient annealing, and (c) the crystal growth at the beginning (Stage I) and in the course of the seeding zone melting experiment (Stage II), and a typical crystal obtained via seeding zone melting.

Fig. 2 Experimentally determined Bi_2Te_3 rich part of the pseudo-binary Bi_2Te_3-In_2Te_3 phase diagram, the

in-set showing backscatterd electron (BSE) microstructure of the complete resolidified mushy zone.

Fig. 3 BSE images and X-ray diffraction patterns of zone-melted $Bi_{40-x}In_xTe_{60}$ ingot after solidification with a pulling rate of 2μm/s and a temperature gradient 5K/mm. The images on the left-hand side correspond to the zone-melted region, and on the right-hand side to the quenched liquid.(a) (b) $Bi_{33}In_7Te_{60}$, without seed alloy; (c) (d) $Bi_{33}In_7Te_{60}$, with seed alloy $Bi_{26.5}In_{13.5}Te_{60}$; (f) X-ray diffraction patterns of $Bi_{33}In_7Te_{60}$ and $Bi_{37}In_3Te_{60}$ samples after seeding zone melting and the standard isotropic XRD pattern of Bi_2Te_3.

Fig. 4 Composition profiles in zone-melted $Bi_{40-x}In_xTe_{60}$ crystals along the growth direction; with a pulling rate of 2μm/s and a temperature gradient 5K/mm. (a) $Bi_{33}In_7Te_{60}$, no seed; (b) $Bi_{33}In_7Te_{60}$; with seed alloy $Bi_{26.5}In_{13.5}Te_{60}$; (c) $Bi_{37}In_3Te_{60}$,with seed alloy $Bi_{33}In_7Te_{60}$.

Table 1 Comparison between Czochralski, Bridgman, zone melting (without seed) and seeding zone melting methods of producing single crystals. Simplified theory is used to illustrate how the final concentration distribution differs. Here the case of systems with initial alloy concentration of C_0 and a solute distribution coefficient (k) lower than 1 (which is the case of Bi_2Te_3-In_2Te_3) is used.

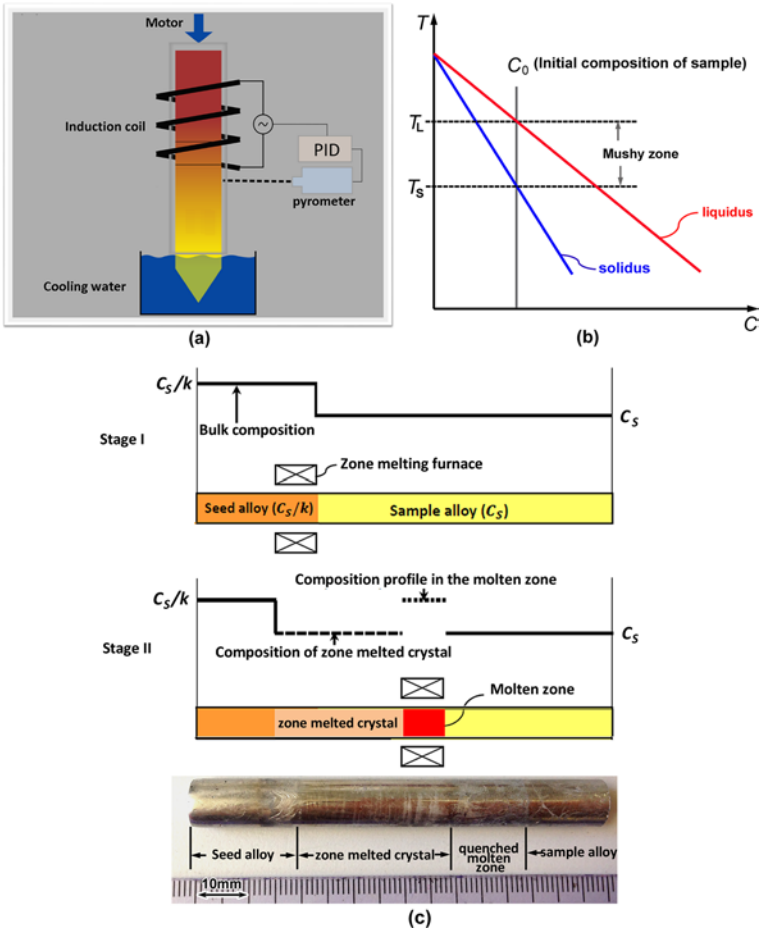

Fig. 1 Schematic illustrations of (a) experimental set-up and (b) determination of phase diagram via temperature gradient annealing, and (c) the crystal growth at the beginning (Stage I) and in the course of the seeding zone melting experiment (Stage II), and a typical crystal obtained in an interrupted seeding zone melting experiment.

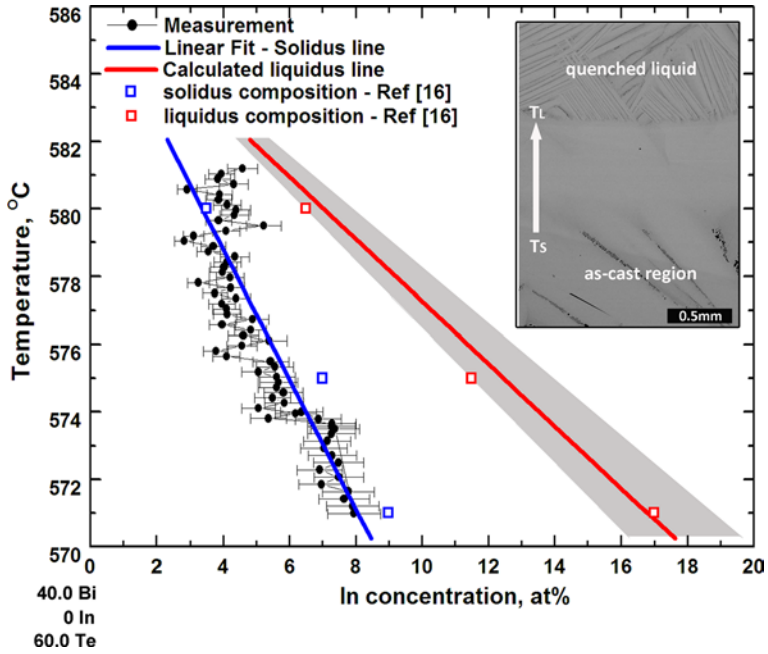

Fig. 2 Experimentally determined solidus line and liquidus line in the Bi_2Te_3 rich part of the pseudo-binary Bi_2Te_3-In_2Te_3 phase diagram, the in-set showing backscatterd electron (BSE) microstructure of the complete resolidified mushy zone.

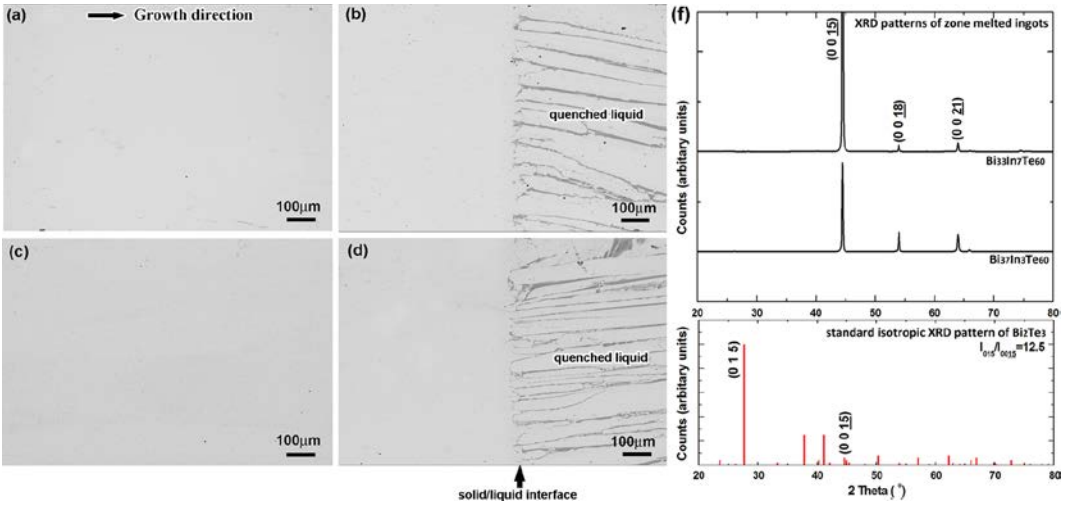

Fig. 3 BSE images and X-ray diffraction patterns of the zone-melted $Bi_{40-x}In_xTe_{60}$ ingot after solidification with a pulling rate of 2μm/s and a temperature gradient 5K/mm. The images on the left-hand side correspond to the zone-melted region, the ones on the right-hand side to interface to the quenched liquid. (a) (b) $Bi_{33}In_7Te_{60}$, without seed alloy; (c) (d) $Bi_{33}In_7Te_{60}$, with seed alloy $Bi_{26.5}In_{13.5}Te_{60}$; (f) X-ray diffraction patterns of $Bi_{33}In_7Te_{60}$ and $Bi_{37}In_3Te_{60}$ samples after seeding zone melting and the standard isotropic XRD pattern of Bi_2Te_3.

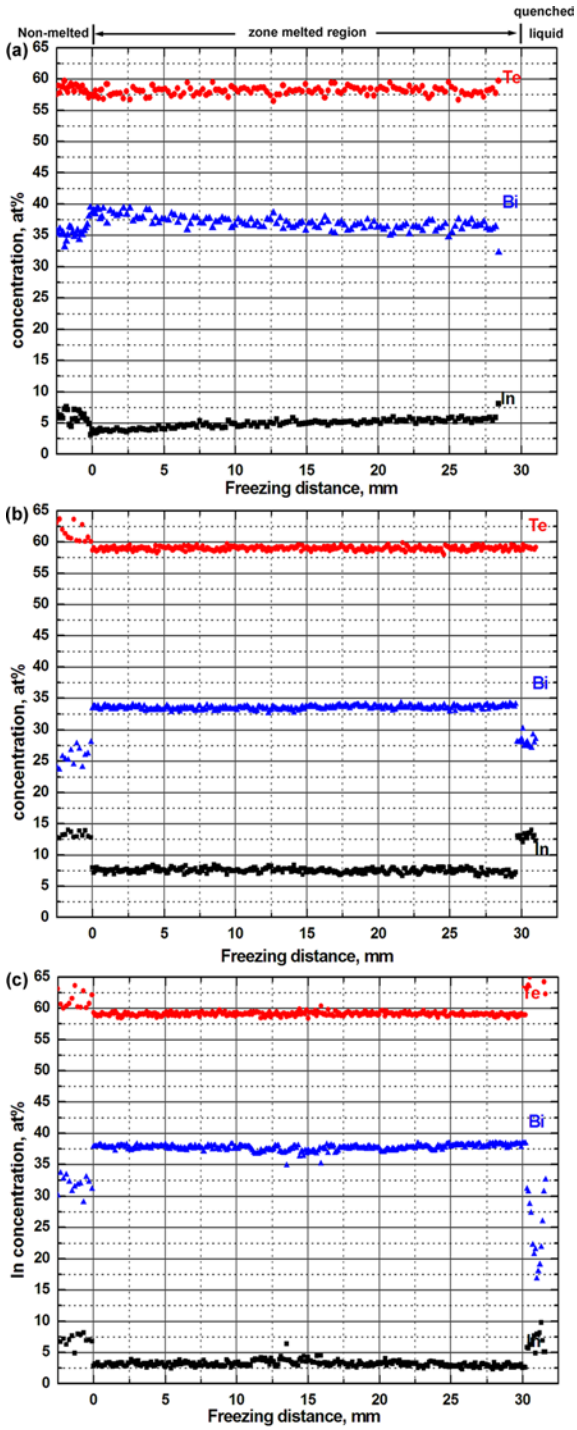

Fig. 4 Composition profiles in zone-melted $Bi_{40-x}In_xTe_{60}$ crystals along the growth direction; with a pulling rate of 2μm/s and a temperature gradient 5K/mm.

(a) $Bi_{33}In_7Te_{60}$, no seed; (b) $Bi_{33}In_7Te_{60}$; with seed alloy $Bi_{26.5}In_{13.5}Te_{60}$; (c) $Bi_{37}In_3Te_{60}$, with seed alloy $Bi_{33}In_7Te_{60}$.

Table 1 Comparison between Czochralski, Bridgman, zone melting (without seed) and seeding zone melting methods of producing single crystals. Simplified theory is used to illustrate how the final concentration distribution differs. Here the case of systems with initial alloy concentration of C_0 and a solute distribution coefficient (k) lower than 1 (which is the case of Bi_2Te_3-In_2Te_3) is used.

Method	mass transport in melt	Composition distribution in the grown crystal	Ref
Czochralski	convection	Initial concentration $kC_0\rightarrow$ continually increasing (length of concentration gradient depending on melt volume)$\rightarrow$initial and final transients are connected	[8,9]
Bridgman	diffusion/convection	Initial concentration $kC_0\rightarrow$ continually concentration increasing till $C_0\rightarrow C_0$ during steady-state growth$\rightarrow$concentration increasing during final transients (length of initial transient depending on growth speed and great increase in presence of convection)	[10,11]
Zone melting	diffusion/convection		[5-7]
Seeding zone melting	convection	C_0 across the whole grown crystal	Present work

A tailored seeding zone melting aiming to synthesize oriented Bi-In-Te crystals with enhanced chemical homogeneity is reported.